Some Concepts in Reaction Dynamics

JOHN C. POLANYI

The objective in this work has been one which I have shared with the two other 1986 Nobel lecturers in chemistry, D. R. Herschbach and Y. T. Lee, as well as with a wide group of colleagues and co-workers who have been responsible for bringing this field to its current state. That state is summarized in the title; we now have some concepts relevant to the motions of atoms and molecules in simple reactions, and some examples of the application of these concepts. We are, however, richer in vocabulary than in literature. The great epics of reaction dynamics remain to be written. I shall confine myself to some simple stories.

Experimental and Theoretical Approaches

In this section I shall discuss the experimental and theoretical tools we have used, and give an indication of their origins. Our principal experimental method has been the study of infrared (IR) chemiluminescence. The most valuable theoretical tool has been and continues to be the computer integration of the classical equations of motion. Although both of these methods belong to the modern period of reaction dynamics, both have clear antecedents in earlier times.

IR chemiluminescence derives from the presence of vibrationally excited molecules in the products of reaction. Indirect evidence for the existence of such species was obtained by M. Polanyi and co-workers in 1928 in the course of studies of the reactions of alkali metal atoms and halogens (*1*). Following a suggestion by Bates and Nicolet (*2*) and by Herzberg (*3*), McKinley, Garvin, and Boudart (*4*) looked for and found visible emission from vibrationally excited hydroxyl radicals that were formed in the reaction of atomic hydrogen with ozone. This finding was soon followed by the identification by absorption spectroscopy of vibrational excitation in the products of the reactions of atomic oxygen with NO_2 and ClO_2 (*5*).

In the same year that (*5*) appeared, we began a search (in collaboration with J. K. Cashion) for IR chemiluminescence from vibrationally excited hydrogen halides (and other hydrogen-containing compounds) that were formed in simple exchange and addition reactions. The first reaction we studied was that of atomic hydrogen with molecular halogens (*6*, *7*). IR emission observed in the region from 1.5 to 4.5 μm arose from the low-pressure ($\sim 10^{-1}$ torr) room-temperature reaction

$$H + X_2 \rightarrow HX^\dagger + X \qquad (1)$$

where X was Cl or Br.

At that time there was lively discussion of the possibility of a visible analogue of the maser that would operate on population-inverted electronic states (a working laser was still in the future) (*8*). Given our interests, it was natural to speculate about the properties of a vibrational laser. In our communication ("Proposal for an infrared maser dependent on vibrational excitation") (*9*, *10*) we indicated a number of virtues of such a device of which I shall note two here. (i) Provided that the vibrational temperature T_V sufficiently exceeded the rotational temperature T_R (both temperatures being positive, in contrast to the negative temperatures associated with population inversion in the discussions of that date), a large number of *P*-branch transitions would exhibit population inversion (Fig. 1). We named this phenomenon "partial population inversion" and noted that lasing based on partial population inversion could ensue shortly after a thermal pulse (arising from a pulsed arc or a shock wave), since "partial cooling" would ensure that $T_V >> T_R$. (ii) A chemical reaction could be used to obtain either "partial" or "complete" population inversion. We were struck by the fact that the upper atmosphere could constitute a natural laser in the infrared that was favored by its long path length and a large number of partial population inverted transitions (*9–11*).

Vibrational lasing was first achieved by Patel and co-workers (*12*). Chemical reaction as the working process in a vibrational laser followed shortly afterward through the work of Pimentel and his associates (*13*). In both cases the major contribution to lasing came from partial population inversion, as indicated by the predominance of *P*-branch emission.

In our first communication regarding IR chemiluminescence we expressed the view that the method "promises to provide for the first time information concerning the distribution of vibrational and possibly rotational energy among the products of a three-center reaction" (*6*, p. 456). This outcome was not so readily achieved.

By 1962 it was evident that the reaction in Eq. 1, despite the fact that it had proved to be a ready source of IR chemiluminescence, converted its heat of reaction into vibration with the modest efficiency of $\leq 50\%$ (*14*). This finding was met with skepticism, since it was correctly pointed out that such conversion implied that the reverse endothermic process could have so much vibration in the reagents that the reaction probability would be markedly diminished (*15*). The somewhat lame reply at that date was that "though odd, it could still be the case" (*16*, p. 279).

Today we would surmise that it is the case, since for the endothermic process $Cl + HCl \rightarrow Cl_2 + H$, a heavy particle (Cl) must approach during the brief time that the H–Cl bond remains extended; too much vibrational excitation can have the consequence that the Cl + HCl interaction is averaged over many vibrational periods, resulting in an "adiabaticity" with respect to the flow of energy into the bond about to be broken. At that time the importance of the relative timing of molecular motions (though

---

The author is professor of chemistry at the University of Toronto, Toronto, Canada M5S 1A1. This article is a condensed version of the lecture he delivered in Stockholm, Sweden, 8 December 1986, when he received the Nobel Prize in Chemistry, which he shared with Dudley R. Herschbach and Yuan T. Lee. It is published here with the permission of the Nobel Foundation and will also be included in the complete volume of *Les Prix Nobel en 1986* as well as in the series *Nobel Lectures* (in English) published by Elsevier Publishing Company, Amsterdam and New York. Drs. Herschbach's and Lee's lectures will appear in forthcoming issues.

recognized for other types of inelastic encounters) had not yet been documented for chemical reactions. We would later illustrate this in a computer animated film (*17*).

It was not until 1967, with the development of the methods of "measured relaxation" (MR) (*16*) and "arrested relaxation" (AR) (*18*), that the goals established 9 years earlier were truly achieved. The impediment to obtaining full quantitative data by IR chemiluminescence, or any other means, in regard to what we have termed the "detailed rate constants" $k(V',R')$ (V' is the product vibrational excitation, and R' the product rotational excitation) had been the presence of an undetermined amount of vibrational and rotational relaxation of the reaction product prior to observation.

In the MR approach (*18, 19*) this was addressed by measuring the vibrational relaxation at points along the direction of flow, and hence correcting for this effect. In the AR method (*18, 20–23*), relaxation, rather than being measured, was arrested to the fullest extent possible by the rapid removal of excited products. This was achieved by complete deactivation at a surface that was usually cooled in the range from 20 to 77 K. Arrest of relaxation yielded detailed rate constants at the level $k(V',R',T')$, where T' is the translational energy distribution in the newly formed product, obtained by subtracting the initial vibrational plus rotational distributions from the total available energy.

Concurrently with the development of these IR chemiluminescence techniques, the crossed–molecular beam method was established as a quantitative tool, particularly by Herschbach and co-workers. This method, which was the outgrowth of work in a number of laboratories, obviated problems of relaxation by conducting the reaction under single-collision conditions. Since the prime measurables were angular and translational energy distributions of the products, by 1967 a degree of overlap existed between the approaches. It was not, however, until the incorporation of universal detectors by Lee and Herschbach, following what we have come to know as the "alkali age" of beam chemistry, that the same systems could be studied by both IR chemiluminescence and molecular beam scattering.

By the time the first quantitative data began to appear, powerful theoretical tools were available that could be used to link the potential field operating between atoms A, B, and C in a reaction

$$A + BC \rightarrow AB + C \qquad (2)$$

to the motions of the particles. In the original work on the London equation (*24*) by Eyring and Polanyi (*25*) an attempt was made, in collaboration with Wigner, to solve the classical equations of motion for the reactive system A + BC. This work was taken up by Hirschfelder and Wigner (*26*), but it was not until the first computer calculations of reaction dynamics by Wall, Hiller, and Mazur (*27*) that the full power of the approach became evident.

In parallel with Blais and Bunker (*28*) our laboratory (*29*) used the approach of Wall, Hiller, and Mazur in an attempt to map out the major determinants of A + BC reaction dynamics. Both groups were inspired by the proposal made by Evans and Polanyi (*30*) over two decades earlier that vibration in a newly formed bond might originate from the release of reaction energy as the reagents approached. Detailed computation indicated that this suggestion embodied an important kernel of truth, although the full story, as might have been expected, revealed a substantially richer range of scenarios.

Energy Distribution Among Reaction Products

Experiment. In the MR method several observation windows for recording IR chemiluminescence were located along the line of streaming flow. Provided that the observation windows were situated at distances corresponding to times during which relaxation was moderate, a simple graphical extrapolation back to zero time yielded adequate values for the relative $k(v')$ (v' is the vibrational quantum number corresponding to the product vibrational energy V') (*18, 19*). Detailed numerical analyses were also made that included the effects of reaction, diffusion, flow, radiation, and collisional deactivation (*19*). A model of this sort permitted, in effect, a more intelligent extrapolation to time $t = 0$.

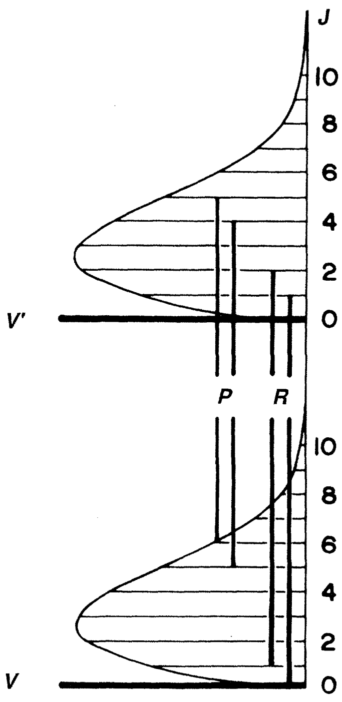

Fig. 1. "Partial population inversion." The condition $T_{\mathrm{V}} >> T_{\mathrm{R}}$ (>0) ensures that the population in the upper state N_{u} exceeds that in the optically linked lower state N_{l} for the indicated transitions (among others). The condition for lasing, $(N_{\mathrm{u}}/g_{\mathrm{u}}) > (N_{\mathrm{l}}/g_{\mathrm{l}})$, where g is degeneracy, is only met for the *P*-branch. [Courtesy of *Applied Optics, Supplement* (*11*)]

Subsequently the flow-tube approach was applied to the determination of vibrational energy distributions in a substantial number of IR chemiluminescent reactions, particularly by Setser and co-workers (*31*) and by Kaufman and co-workers (*32*). Studies of IR chemiluminescence in flow tubes have also been extended to the elucidation of product energy distributions from ion-molecule reactions (*33*).

In the AR method two uncollimated beams of reagents met in the center of a vessel that exhibited a background pressure (with the reagents flowing) of $\sim 10^{-4}$ to 10^{-5} torr. The reaction occurred at the intersection of the beams [as demonstrated in (*20*)]. The products of reaction were transferred, after a few secondary collisions, to a deactivating surface which surrounded the reaction zone. Depending on the reagents, this surface acted as a cryopump, as a getter pump (trapping noncondensibles in excess condensible), or simply as an adsorber capable of bringing about complete vibrational deactivation (by adsorbing the product for a time sufficient to deactivate the material to its ground vibrational state $v = 0$).

The IR chemiluminescence stemming from the small fraction of molecules that emitted early in their lifetimes was collected by mirrors; this procedure increased the effective solid angle being viewed by almost a factor of 50 (*34*). By this means $\sim 10^{-9}$ torr of vibrationally excited product could be detected in one v,J (vibrotational) state.

The AR method was adopted by several laboratories, notably those of Jonathan (*35*), Setser (*36*), and McDonald (*37, 38*). It is characterized by molecular flow of the reactants and hence low densities in the reaction zone that permit observation of reaction products with highly non-Boltzmann rotational distribution as well as non-Boltzmann vibrational distributions.

The effectiveness of the combination of molecular flow plus rapid removal of reaction products in reducing relaxation to an insignificant amount in the majority of systems studied was indicated by the fact that the steady-state distribution observed under these conditions was in satisfactory agreement with the initial vibrational distribution obtained by the MR method, and that the observed rotational distribution was largely unrelaxed, indicating that collisional deactivation of vibrators, which is generally a less efficient process, was insignificant. In the case of a few very fast reactions [notably $F + HBr \rightarrow HF + Br$ (*31*)] $k(v')$ from MR were at variance with those from AR. At the low flows used in the AR instrument it appears that reaction and deactivation were occurring within the inlets, which invalidated the results (*39*); in such a case the AR rotational distributions were also found to have been relaxed (*40*).

Detailed rate constants, $k(v')$, for the reaction

$$F + H_2 \rightarrow HF + H \qquad (3)$$

obtained by different procedures and by different workers over the period from 1969 to 1984 can be compared. Among the methods used was one due to Pimentel and co-workers that made use of stimulated, rather than spontaneous, IR emission (*41*). This approach was an outgrowth of the first chemical laser developed in the same laboratory (*13*). The laser approach (*41*) gave quantitative data concerning the population in the vibrational ground state $v' = 0$, which previously had been unobservable. A set of $k(v')$ values has also been obtained from crossed–molecular beam studies by Y. T. Lee and co-workers (*42*). In these demanding experiments the vibrational distribution was obtained from structure in the product translation energy distribution, which was the measured quantity. The agreement between determinations of $k(v')$ was satisfactory.

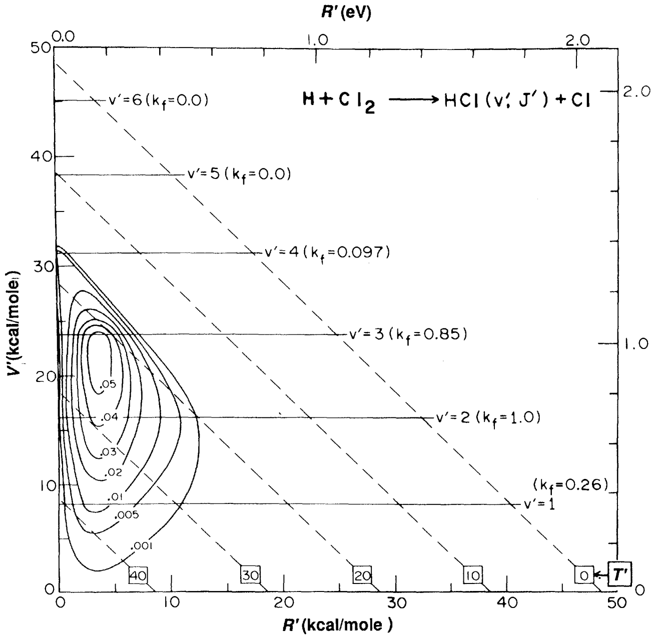

Fig. 2. Triangle plot for $H + Cl_2 \rightarrow HCl + Cl$ reaction showing the distribution of vibrational, rotational, and translational energy as contours of equal detailed rate constant $k(V',R',T')$. The ordinate is product vibrational energy, and the abscissa is the product rotational energy. Since the total available energy is approximately constant (E'_{tot} = 48.4 kcal/mole), the translational energy T', given by the broken diagonal lines, increases to 34 kcal/mole at $V' = 0$, $R' = 0$. The rate constant $k_f \equiv k(v') = \Sigma_{J'}k(v',J')$; the subscript f denotes the "forward," exothermic direction. Contours have been normalized to $k(\hat{v}') = 1.00$, where $\hat{v}'$ is the most populated vibrational level. [Courtesy of *The Journal of Chemical Physics* (*21*)]

At the time that these experiments and those described below were undertaken, quantitative data regarding $k(v')$ did not exist. The prior observation of highly vibrationally excited reaction products noted above was a qualitative finding, and left open the question of the form of $k(v')$, which could have peaked anywhere from $v' = 0$ to $v' = v'_{max}$ (the highest accessible vibrational state). In fact, the distributions observed by IR chemiluminescence were found to peak at intermediate v', so that the mean fraction of the available energy entering vibration in the new bond ranged from $\langle f'_V \rangle = 0.39$ for

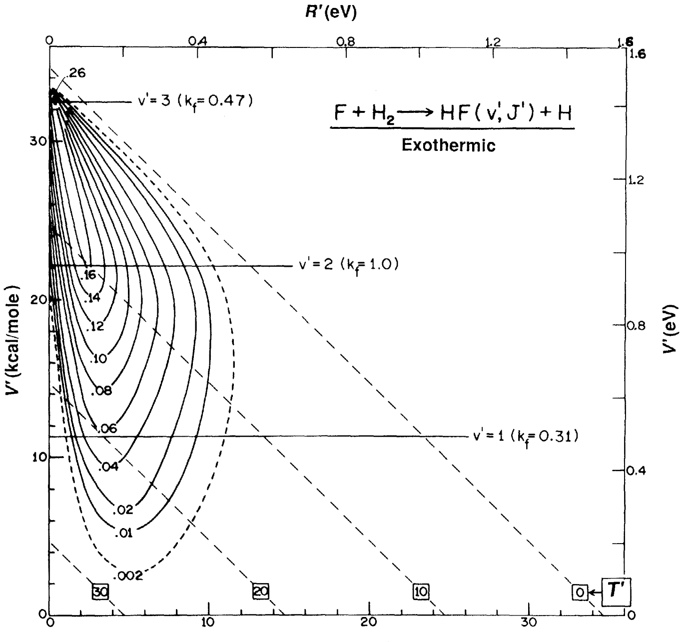

Fig. 3. Triangle plot for $F + H_2 \rightarrow HF + H$ (see caption to Fig. 6). E'_{tot} = 34.7 kcal/mole for this reaction. [Courtesy of *The Journal of Chemical Physics* (*22*)]

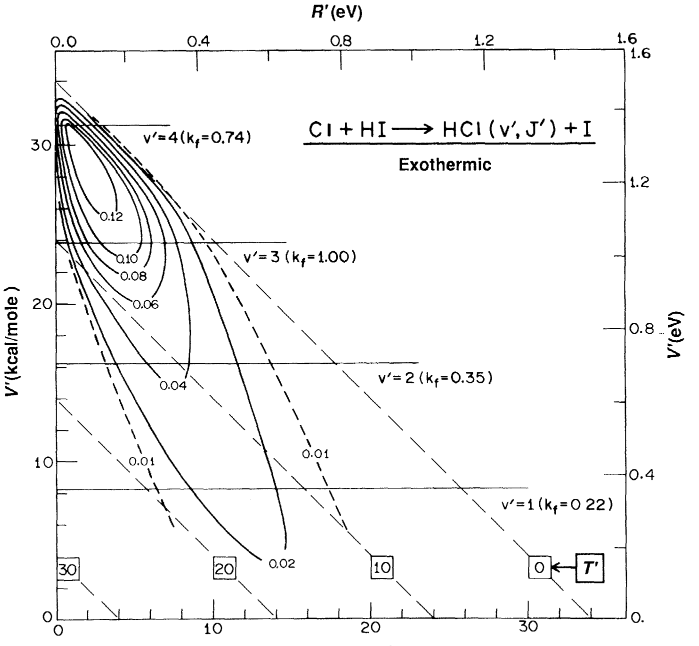

Fig. 4. Triangle plot for $Cl + HI \rightarrow HCl + I$. See caption to Fig. 7. E'_{tot} = 34 kcal/mole. [Courtesy of *The Journal of Chemical Physics* (*20*)]

$H + Cl_2$, $\langle f'_V \rangle = 0.55$ for $H + Br_2$, $\langle f'_V \rangle = 0.53$ for $H + F_2$, $\langle f'_V \rangle = 0.66$ for $F + H_2$, and up to $\langle f'_V \rangle = 0.71$ for $Cl + HI$ and $\langle f'_V \rangle \approx 0.9$ for $H + O_3 \rightarrow OH + O_2$.

Three examples of the graphs that we have used [as a supplement to the tabulation of the actual $k(v',J')$ values] as an aid to the visualization of the experimentally determined product energy distributions are shown in Figs. 2 through 4. By interpolation between permitted combinations of V', R', and T', we obtain contours of equal $k(V',R',T')$. In these "triangle plots," contours are shown in V',R',T' space. They delineate a "hill" of detailed rate constant in that space. Portions of the hill that lie between vibrational energy states are merely included to guide the eye as to the breadth and shape of the product energy distribution over the axis corresponding to V', R', and T'. Since classical mechanics is widely used to interpret energy distributions, these classical "fingerprints" of differing chemical reactions help us to picture contrasting types of behavior.

It is readily apparent that the first reaction, $H + Cl_2$ (Fig. 2), exhibits inefficient vibrational and rotational excitation and consequently efficient translational excitation. The second reaction, $F + H_2$ (Fig. 3), gives rise to highly efficient vibrational excitation together with inefficient rotational excitation. The third reaction pictured, $Cl + HI$ (Fig. 4), combines efficient vibrational excitation with exceptionally efficient rotational excitation. In concurrent work alluded to in the following section, we linked these changes in dynamics to the release of repulsive energy in systems that have differing mass combination and preferred geometries of the intermediate.

The ridge of the "detailed rate constant hill" is almost vertical in the case of the first two reactions, moving out to higher R' at lower V' in the third of the reactions pictured ($Cl + HI$). Successively lower vibrational states therefore exhibit marked increases in translational energy in the first two cases, but a somewhat overlapped "translational energy spectrum" in the third case. This finding was seen to have interesting implications for the crossed–molecular beam chemistry, in which T' is the prime measurable. Figure 5 gives sample distributions over f'_T [blending rotational states into a continuum, since they cannot be resolved in molecular beam time-

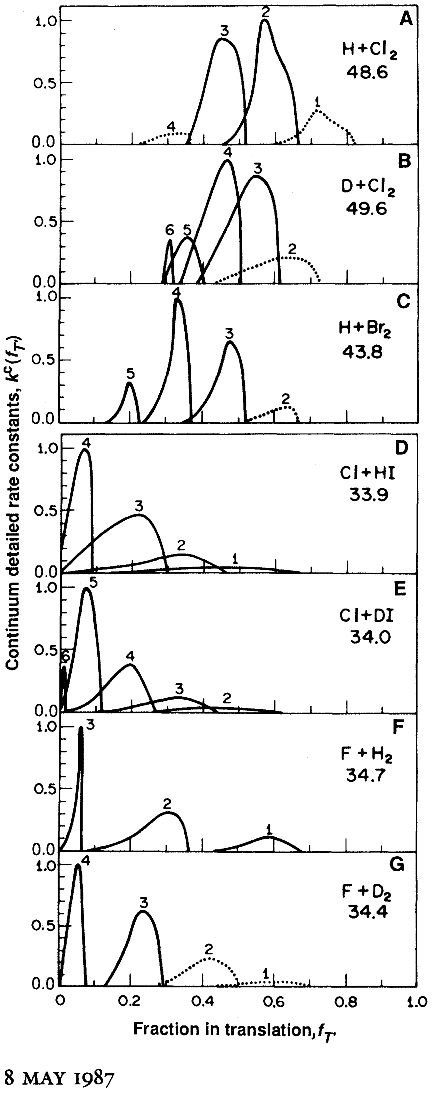

Fig. 5. Translational energy distribution in the products of some exchange reactions $A + BC \rightarrow AB + C$ obtained by subtracting the vibrational excitation measured by IR chemiluminescence from the total product energies (indicated in the figure). The vibrational states that contribute to the translational peaks are recorded above each peak. [Courtesy of *The Journal of Chemical Physics* (45)]

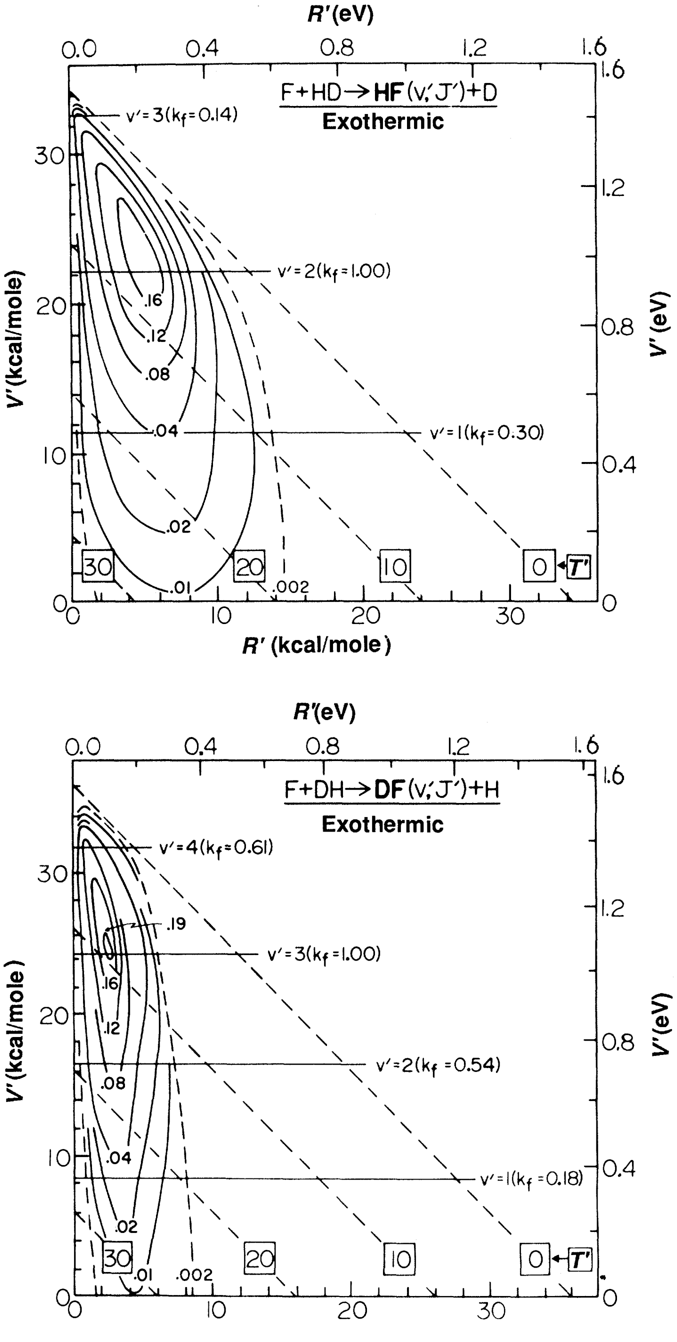

Fig. 6. Triangle plots for both branches of the F + HD exchange reaction. The total available energy in the products was taken to be $E'_{tot} = 34.3$ kcal/mole for the HF product, and $E'_{tot} = 36.1$ kcal/mole for DF, in calculating product translation T'. [Courtesy of *Chemical Physics* (44)]

of-flight (TOF) studies]. In the case of the F + H_2 reaction and its isotopic analogues, in addition to resolving these peaks by TOF, Y. T. Lee and co-workers have recently fully characterized the angular distribution of each (*42*).

The triangle plots, exemplified in Figs. 2 through 4, constitute one way of "compacting" the substantial data embodied in $k(v',J',T')$. The information-theory approach pioneered by Bernstein and Levine (*43*) has provided a widely used alternative method of compaction in terms of parameters that describe the deviation of the observed vibrational and rotational distributions from a statistical outcome.

Figure 6 contrasts the triangle plots for HF (Fig. 6A) and DF (Fig. 6B) formed in the thermal reaction F + HD → HF(v',J') or DF(v',J') (+ D or + H) (*44*). The forces operating are very similar but clearly are substantially more effective in rotationally exciting HF (mean fraction of the available energy entering rotation is $\langle f'_R \rangle = 0.125$) than DF ($\langle f'_R \rangle = 0.066$). This will be discussed in the section below dealing with theory.

Figure 7 shows the dramatic influence that atom C can have on the dynamics of a reaction A + BC → AB + C. Superficially the reaction illustrated resembles H + ClY → HCl + Y, for which the detailed rate constant $k(V',R',T')$ is given in Fig. 2; the difference is that the second halogen atom Y has been changed from Y = Cl to Y = I, the effect on $k(V',R',T')$ is shown. Bimodal product energy distributions were also observed in a number of other studies (*45–51*) and were regarded as indicative of the existence of two types of reaction dynamics leading to the identical product (HCl in the case illustrated). This phenomenon was termed "microscopic" branching, to distinguish it from the "macroscopic" branching that leads to chemically different products (see, for example, Fig. 6). These two types of branching are linked.

Theory. Figure 8 shows three potential-energy surfaces (PESs), all of a modified London, Eyring, Polanyi, and Sato (LEPS) variety (*29, 52, 53*), selected from a wider group examined in (*53*). The energy released as the reagents approached (termed the attractive energy release, and defined as $\mathcal{A}_\perp$ or $\mathcal{A}_T$ (*47, 48*); see the caption of Fig. 8) increases as one moves upward in the figure. In related families of reaction there is a concurrent diminution in the height of the energy barrier, and a shift of the barrier to earlier locations along the coordinate of approach with increased $\mathcal{A}$. It has proved possible to give an empirical expression to these correlations (*55, 56*).

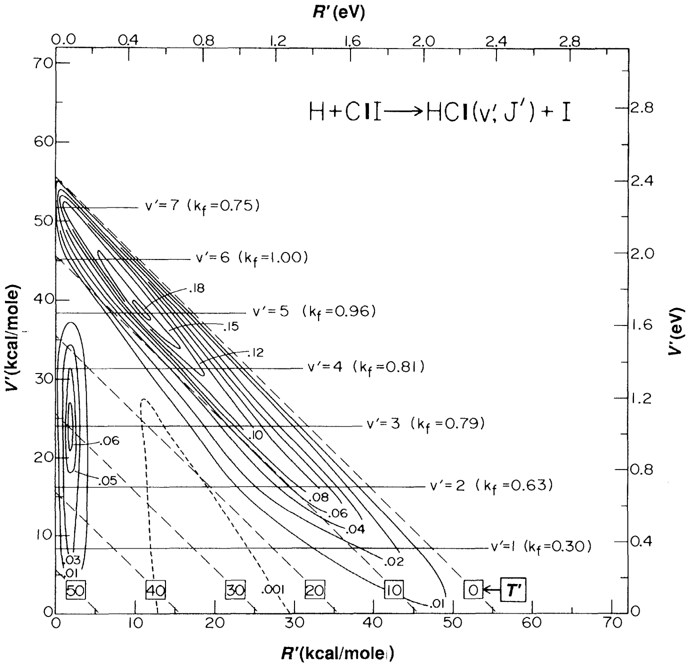

Fig. 7. Triangle plot for the reaction H + ClI at 300 K showing bimodality (18% of the HCl is in the low-J' mode, 82% in the high-J' mode). [Courtesy of *Chemical Physics Letters* (*47*)]

It was found that for a substantial group of PESs (*53*) moderate percentages of energy release along the coordinate of approach (% $\mathcal{A}_\perp$) were converted quantitatively into product vibration for the **L+HH** reagent mass combination. For reactions with high % $\mathcal{A}_\perp$ the reactions moved into a new regime in which product vibration decreased with increased attractive energy release. Examination of the trajectories indicated that a transition had occurred from predominantly direct reaction [reactions in which the products, once they start to separate, continue to do so (*57*)] to indirect reaction [in which subsequent "clutching" and "clouting" secondary encounters drain the incipient vibration out of the new bond into rotation and translation (*58, 59*)]. What we were seeing was the onset of statistical behavior, in the limit of which product vibration would receive no more than its modest equipartition allocation.

At the end of the scale in which repulsive energy release predominated, low vibrational excitation was by no means the general rule; the observed vibrational excitation was strongly dependent on the

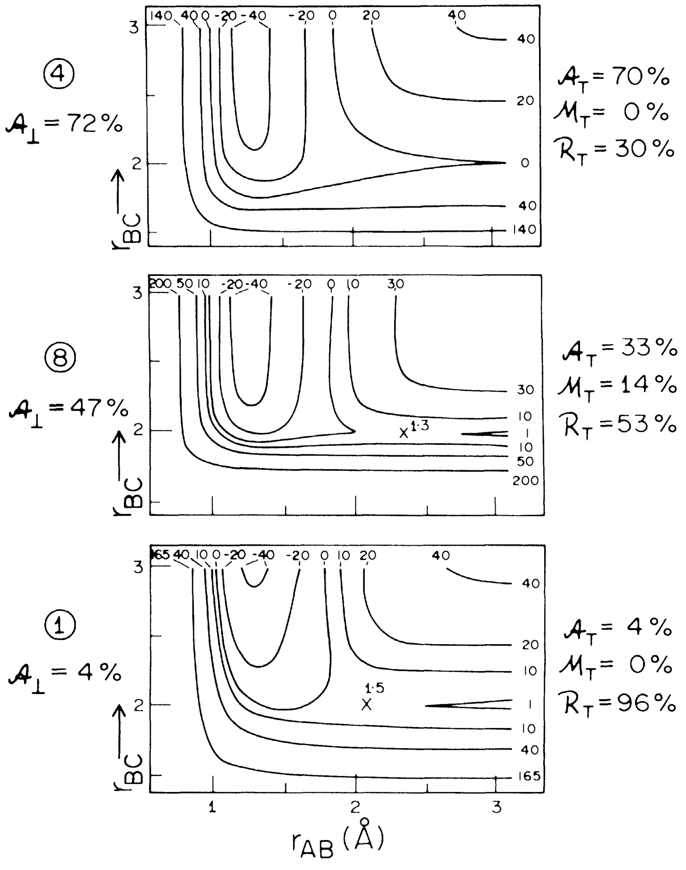

Fig. 8. Three PESs that illustrate changes in potential energy as reagents A + BC (lower right) pass through collinear transition states A--B--C to form products AB + C (upper left). Contour energies are in kilocalories per mole; all three reactions have the same exothermicity. The PESs, designated 1, 8, and 4, are arranged vertically in order of increasing "attractiveness." The PESs are indexed at the left according to the percentage attractive energy release taken from a perpendicular path across the surface ($A_\perp$ = 4, 47, and 72% for surfaces 1, 8, and 4). The same PESs are described at the right according to the percentages attractive, mixed, and repulsive energy release $\mathcal{A}_\perp$, $\mathcal{M}_T$, and $\mathcal{R}_T$ along a single collinear trajectory; this designation depends on mass combination, which was **L+HH** (**L** has a mass of 1 amu, and **H** has a mass of 80 amu). The barrier crest, designated **x**, shifts to "earlier" locations along r_{AB} as the surfaces become more attractive. [Courtesy of *The Journal of Chemical Physics* (*53*)]

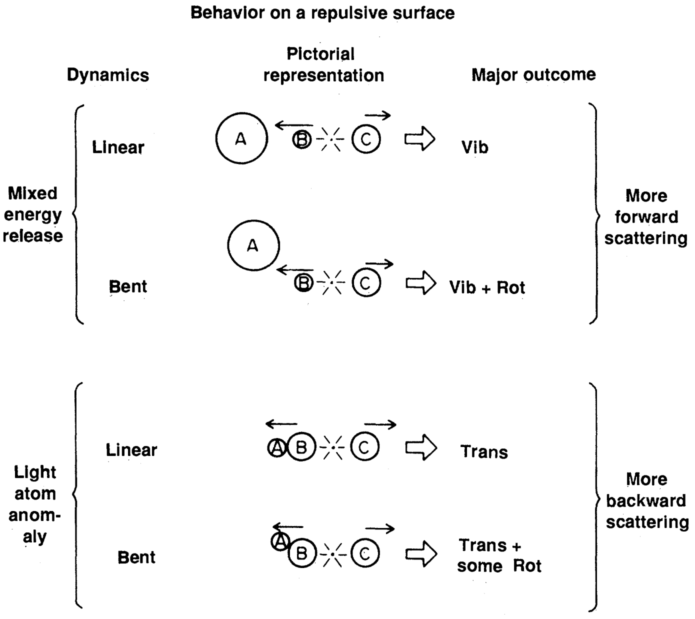

Fig. 9. Pictorial representation of contrasting types of reaction dynamics on a repulsive energy surface. "Mixed energy release," is commonly observed. "The light-atom anomaly" is observed if the attacking atom is very light. [Courtesy of *Accounts of Chemical Research* (*58*)]

chosen mass combination. The **L+HH** mass combination is in fact anomalous in fulfilling the initial expectation that repulsive energy release $\mathcal{R}_\perp$ (energy released along the coordinate of separation of the PES) will be inefficiently channeled into vibration. For **L+HH** the attacking atom A approaches BC rapidly up to the normal bonding separation before the repulsion is released (dynamics in which the interatomic distance r_{AB} decreases to its equilibrium separation r^0_{AB}, and only then does r_{BC} increase, which corresponds on the PES to a rectilinear path). Since the repulsion operates on an already existent A–B bond, vibrational excitation is indeed inefficient. This behavior was sufficiently atypical to be described as the "light-atom anomaly" (*53*).

For the more general case of a heavier attacking atom relative to the molecule under attack, the new bond is still extended ($r_{AB} > r^0_{AB}$) at the time that the bulk of the repulsion is released; we can symbolize this as A- -B ▪ C. In this case repulsion between the separating atoms B and C results in recoil of B, rather than of AB as a whole, that is, it gives rise to efficient internal excitation of the new bond A–B.

Since the solution of the collinear equations of motion can be pictured in terms of the motion of a mass sliding across a suitably scaled and skewed representation of the PES, it is instructive to consider the characteristic path across the PES in the latter, more general case. The fact that r_{AB} decreases at the same time as r_{BC} increases (we term the energy released in this phase "mixed" or $\mathcal{M}$) means that the sliding mass, rather than following a rectilinear path, is cutting the corner of the PES. Therefore, instead of approaching the exit valley from its head, it approaches the valley from the side; consequently it oscillates from side to side of the exit valley, indicating that the new bond is vibrationally excited.

The proportion of the energy released during corner cutting is clearly relevant to the efficiency with which the repulsive energy is channeled into vibration. We have determined the extent of mixed energy release $\mathcal{M}_T$ from a specimen collinear trajectory that used the appropriate mass combination and the PES in question (*11, 53, 60*). Figure 8 shows that % $\mathcal{M}_T$ is insignificant for **L+HH**. For other mass combinations it is large.

If we turn to the experimental findings discussed above, the evidence favors strongly repulsive PESs, with the light-atom anomaly explaining both the markedly reduced $\langle f'_v \rangle$ for $H + X_2$ as compared with $X + H_2$ or $X + HY$, and the lower barrier leading to a slightly increased $\mathcal{A}_\perp$ in $H + Br_2$ as compared with $H + Cl_2$ (compare with the correlation noted above) accounting for the greater $\langle f'_v \rangle$ observed for $H + Br_2$ than for $H + Cl_2$ (*18*). Strongly repulsive PESs have successfully accounted for the general forms of the triangle plots (*61–64*). In the case of $F + H_2$ there is now dependable evidence from ab initio variational treatments of FHH (*65, 66*) that the energy release is indeed substantially repulsive.

The discussion of the previous paragraphs as it relates to repulsive energy release is summarized pictorially in Fig. 9. Actual tests of the validity of PESs are, of course, made by three-dimensional (3-D) trajectories. Product rotational excitation is eliminated from the picture in the collinear world. Although this is a minor constituent of the product energy, it is revealing of the dynamics. In the visualization of Fig. 9, we have included the effect of repulsive energy release in bent configurations as one source of product rotation. The experimental data in the triangle plots of Fig. 6 give persuasive evidence of the significance of this effect in the reaction $F + H_2$. Product repulsion would be expected (*44*) on the basis of momentum conservation to give rise to decreasing $\langle f'_R \rangle$ in the series FH▪D > FH▪H > FD▪D > FD▪H (the square indicates the locus of the repulsion); this is found theoretically, in 3-D trajectory studies, and also experimentally. The triangle plots of Fig. 6 correspond to the extremes of this range of isotopic mass combinations; $\langle f'_R \rangle$ for the FH▪D pathway substantially exceeds that for FH▪H.

Qualitative pictures of the type given in Fig. 9 suggest simple models of the reactive event (*59*). Despite their crudity, simple models have the important virtue that their "moving parts" are open to inspection.

The simple harmonic model (*60*) has been used to improve our understanding of the mechanism of mixed energy release, in which a repulsive force operating between particles B and C drives an oscillator joining A to B that is under tension. The model shows that for a wide range of conditions mixed energy release can play a significant role in channeling product repulsion into vibration.

The DIPR (direct interaction with product repulsion) model (*67*) sidesteps consideration of forces in the new bond by obtaining the product vibration V' from $E'_{tot} - (R' + T')$, where E'_{tot} is the product rotational excitation. From the direction of recoil of atom C relative to the direction of approach of A, angular distributions can readily be generated in three dimensions. The model provides a simple means to expose the link between the angular distribution of reaction products and their internal excitation, as well as the connection between these two quantities and the collision energy.

Findings for the DIPR model are summarized in Fig. 10 (solid lines). The interactions become less repulsive (more attractive) from left to right. This is achieved by systematically decreasing the repulsive impulse [the time integral of the force, $F(t)$, between B and C] which alone governs the dynamics. Since a measure of $\int F(t)\,dt$ can be obtained by a variety of means for any actual reactive PES (*59, 67*), the model can be tested by being applied to cases for which the results of 3-D trajectory computation are known. The agreement is excellent (see the points for the more repulsive cases in Fig. 10), so long as the assumption of direct interaction remains valid.

The lessons that can be learned from Fig. 10 are that strongly repulsive energy release will tend to give backward scattering of the molecular product (θ_{mol} is substantial at 180°) coupled with moderate internal excitation E'_{int}. As the repulsion is decreased, θ_{mol} shifts forward and E'_{int} increases. The same effect can be achieved by increasing the reactant collision energy, since this too has the effect of decreasing the repulsive impulse $\int F(t)\,dt$.

Herschbach and co-workers have injected physical content into

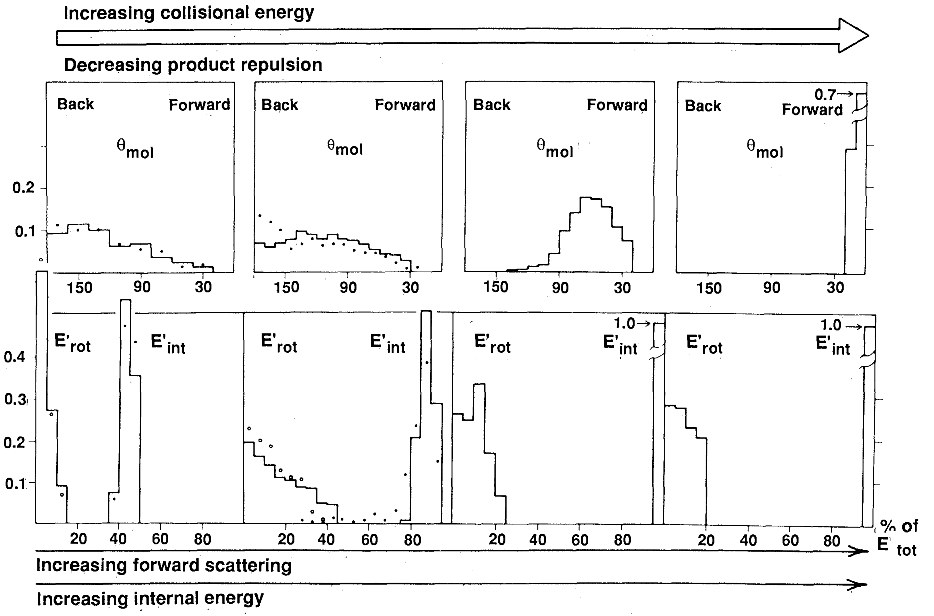

Fig. 10. Effect of repulsive energy release on product angular distribution (top row) and energy distribution (bottom row; E'_{tot} is product rotational excitation and E'_{int} is vibration plus rotation). The solid lines show the results of 3-D DIPR model calculations (masses K + Br_2, energy release E'_{tot} = 53 kcal/mole). The total product repulsion used in the DIPR model calculations was decreased in four stages, from left to right in the figure, which simulated decreased %$\mathcal{R}$, and implied increased %$\mathcal{A}$. According to the DIPR model, this is mathematically equivalent to increasing the reagent collision energy, hence the dual label of the arrow at the top. The consequences of these changes are summarized qualitatively by the arrows at the foot of the figure. The dots record the distributions obtained from 3-D trajectories on potential-energy hypersurfaces with comparable partitioning of the energy release. [Courtesy of *The Journal of Chemical Physics* (*67*)]

the DIPR model in their DIPR–DIP extension, in which the repulsive impulse is assumed to be "distributed as in photodissociation" (*68*). The model then accounts nicely for product distributions observed in a number of reactions. More recently Zare and coworkers have shown how the DIPR approach can be used to understand the plane of rotation of newborn reaction products (*69*).

The FOTO (forced oscillation in a tightening oscillator) model (*70*), gives a fuller rendition of the forces on a collinear PES; the B•C repulsion operates on an AB oscillator whose force constant is increasing and whose equilibrium separation r^0_{AB} is decreasing. The model, which has been applied to ten reactions for which experimental or theoretical data exist, is sufficiently complete to embody analogues of the "attractive," "mixed," and "repulsive" phases of energy release.

To the extent that the rotation in a newly formed reaction product AB originates in repulsion AB•C, the rotational motion should be coplanar with the repulsive force, and B in AB should recoil away from C (Fig. 11). This implies that the angle between the product rotational angular momentum vector **J**′ and the product orbital angular momentum vector **L**′ should be $\theta_{J'L'} \approx 180°$. Analyses of product distributions from 3-D trajectory studies (*64, 71*) bear this out. Experimental studies of correlations between such vector attributes will add materially to the mosaic from which our picture of reaction dynamics is composed.

The richer the detail in the rate constants $k(V',R',T')$, the clearer the message. The striking bimodality in the product energy distribution from H + ClI → HCl(v',J') + I recorded in Fig. 7 can be ascribed to "microscopic branching"; two patterns of molecular dynamics result in the formation of the same reaction product (HCl in this example). The dynamics have been explored in three dimensions for reasonable PESs (*51*). They are shown schematically in Fig. 12. In the case of H + ClI the migratory microscopic pathway (at the right of Fig. 12) is thought to dominate. This is for the same reason that macroscopic branching favors formation of HI rather than HCl, namely, the existence of a smaller energy barrier for approach from the I end of ICl [see (*72, 73*)] for the greater stability of ClIH than HClI. In collisions of H atoms with the I end of ICl that fail to yield HI, the H atom can migrate toward the Cl end of the molecule to yield highly internally excited HCl. The HCl product with low internal excitation comes from H atoms that have reacted directly at the Cl end of ClI. Since the barrier to this mode of reaction is higher, the yield (at normal reagent energies) is lower. It is evident that the relative yields of HCl and HI in macroscopic branching are linked to the yields of low E'_{int} and high E'_{int} HCl by way of microscopic branching.

Microscopic branching is thought to constitute more than merely an interesting curiosity, since it can contribute to the dynamics in any case where macroscopic branching is possible which encom-

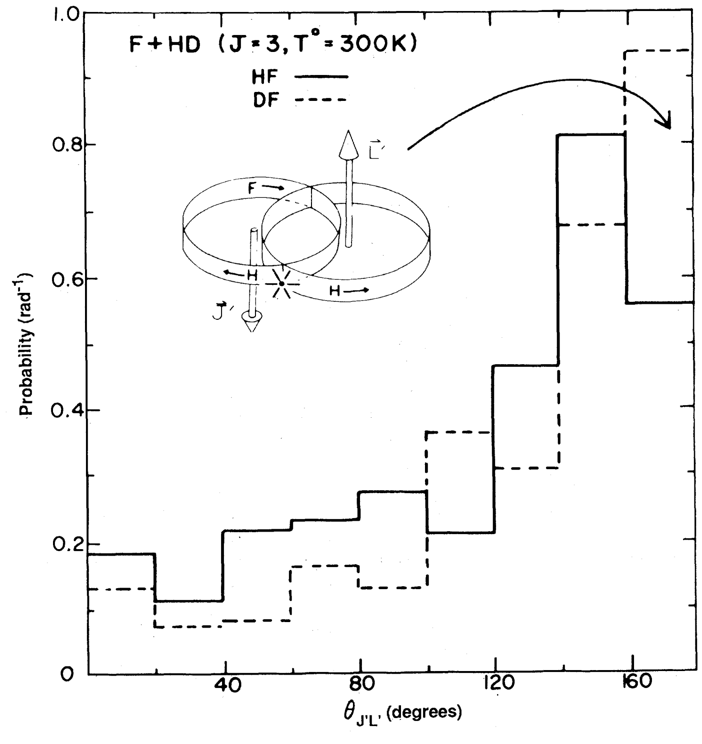

Fig. 11. Computed distribution $\theta_{J'L'}$ of the angle between the product rotational angular momentum **J**′ and orbital angular momentum **L**′ after repulsive energy release between the products of the reaction F + HD → HF + D (solid line) and F + HD → DF + H (broken line). At the extreme left $\theta_{J'L'}$ = 0° corresponds to **J**′ parallel to **L**′, while at the extreme right $\theta_{J'L'}$ = 180° corresponds to the favored outcome of **J**′ antiparallel to **L**′. [Courtesy of *The Journal of Chemical Physics* (*71*)]

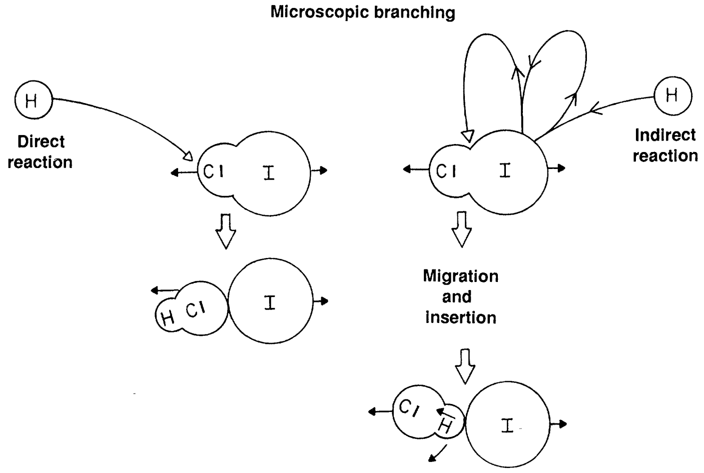

Fig. 12. Pictorial representation of the alternative dynamics, direct and indirect, in the microscopic branching underlying the bimodality of product energy distribution exemplified in Fig. 7. [Based on a classical trajectory study; see (*51*)]

passes a large class of reactions. As would be expected, the importance of microscopic branching, in common with macroscopic branching, is sensitive to the reagent energy (*38, 49, 50*).

Channeling Reagent Energy into Products

Experiment. To increase the collision energy we formed atomic reagents [Cl for Cl + HI (*49*), F for F + HCl or F + D_2 (*50*), and H for H + Cl_2 (*50*)] by pyrolysis rather than using room temperature atoms. The effect is shown for H + Cl_2 in the triangle plot of Fig. 13. Comparison with the earlier 300 K triangle plot (Fig. 2) shows marked changes. The additional reagent translation ΔT in excess of the barrier to reaction has been channeled principally into additional product translation.

A second repository for this additional reagent energy was product rotation. The general finding regarding the disposition of additional reagent translation could be summarized as

$$\Delta T \rightarrow \Delta T' + \Delta R' \qquad (4)$$

This describes the average behavior.

By heating the molecular species under attack, or vibrationally exciting it in a prior reaction (*74*) and recording the change in product energy distribution (see, for example, Fig. 14), we found evidence of a similar adiabaticity, on the average, in regard to the conversion of reagent vibration into product excitation,

$$\Delta V \rightarrow \Delta V' \qquad (5)$$

(the symbol Δ denotes energy in excess of that required for barrier crossing).

Theory. The nature and the origins of the approximate adiabaticity relations (Eqs. 4 and 5) have been discussed in a number of places (*44, 49, 50, 54, 61, 75–78*). The origin of this adiabaticity is evident from an inspection of trajectories with and without the additional reagent energy. The effect of enhanced translation is to shift the characteristic pathway across the collinear PES (used as a diagnostic of 3-D behavior) toward more compressed configurations. The sliding mass impelled by its enhanced momentum along r_{AB} caroms into the corner of the PES region 1 in Fig. 15. If the compressed intermediate A•B•C is collinear, it then flies apart to give translation in AB + C, and, if it is bent, to give enhanced rotation in AB. For enhanced reagent vibration the most common paths to product are shifted to region 2 in Fig. 15; the effect is to favor a more stretched intermediate A- - B- - C that pulls together along r_{AB} to give AB($v >> 0$) + C. The opposite phase of vibration to that pictured in Fig. 15 drives the intermediate into region 1, giving rise to the low V' peak in the product distribution.

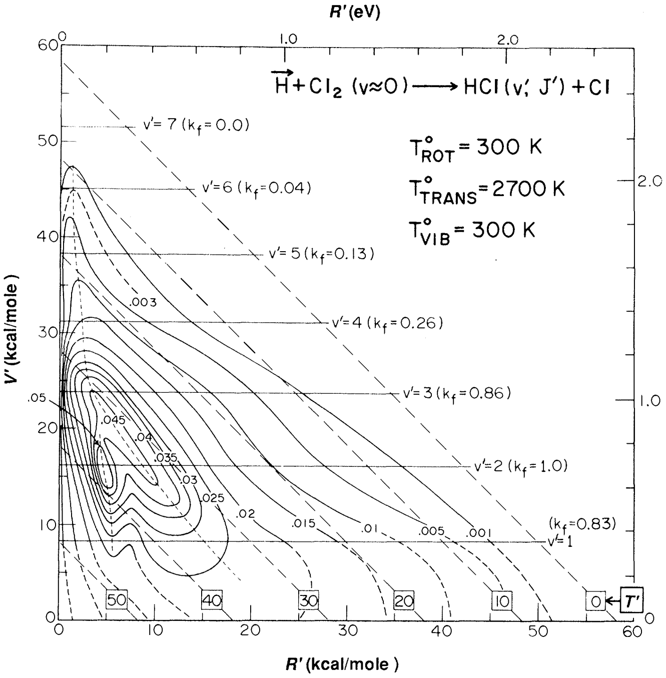

Fig. 13. Effect of enhanced reagent collision energy on the product energy distribution, that is, experimental values of $k(V',R',T')$ for H + $Cl_2(v = 0) \rightarrow HCl(v',J')$ + Cl. Mean collision energy $\langle T \rangle \approx 10.6$ kcal/mole. Compare $k(V',R',T')$ for room temperature reaction in Fig. 6. [Courtesy of *Faraday Discussions of the Chemical Society* (*50*)]

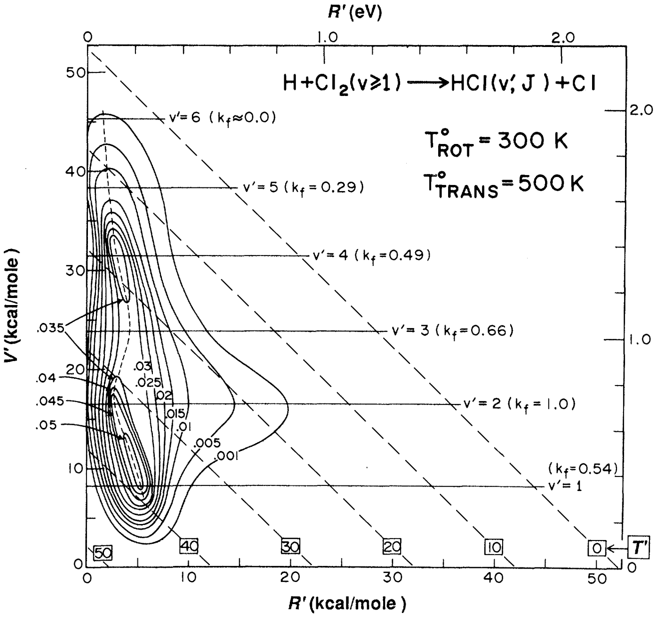

Fig. 14. Effect of enhanced reagent internal energy on the product energy distribution, that is, experimental $k(V',R',T')$ for H + $Cl_2(v \geq 1) \rightarrow HCl(v',J')$ + Cl. This result is approximate since it was obtained by subtracting the detailed rate constants for H + $Cl_2(v \approx 0) \rightarrow$ HCl + Cl from those for H + $Cl_2(v \geq 0) \rightarrow$ HCl + Cl. Mean vibrational energy $\langle V \rangle \approx 3.3$ kcal/mole. Compare with Fig. 2. [Courtesy of *Faraday Discussions of the Chemical Society* (*50*)]

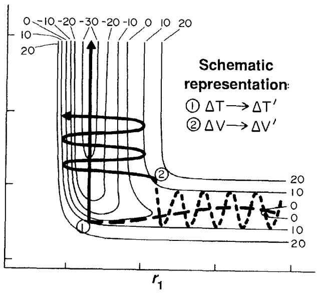

Fig. 15. Schematic representation (on a typical collinear exothermic PES) of the mechanism by which "additional" reagent translation ($\Delta T >> E_c$, where E_c is the barrier height) is channeled into "additional" product translation ($\Delta T'$), and also of the mechanism 2, by which "additional" reagent vibration ($\Delta V >> E_c$) becomes "additional" product vibration ($\Delta V'$). (These are not actual trajectories, since they show neither the exothermic energy release nor the effect on that energy release of changing reagent energy; the intention, which is artificial, is to show the effect of ΔT and ΔV in isolation.) [Courtesy of *Faraday Discussions of the Chemical Society* (*50*)]

Surmounting the Energy Barrier

Experiment. The most detailed information regarding the relative efficiency of various types of reagent motions in surmounting an energy barrier comes from the application of microscopic reversibility to detailed rate constants for the forward reaction $k_f(V',R',T')$ (*79*). Detailed rate constants for the reverse reaction $k_r(V',R',T')$ obtained in this way are recorded in the triangle plot of Fig. 16, where V',R',T' are now the vibrational, rotational, and translational energies of the reagents for the endothermic reaction $HF(v',J') + H \rightarrow F + H_2$ (*80*). The total energy available for distribution is fixed by the nature of the experiment and is equal to the energy made available by the forward exothermic reaction (34.7 kcal/mole in the case illustrated). [This approach has been tested numerically by applying it to a case where $k_r(V',R',T')$ could be obtained directly from 3-D trajectories (*81*)]. Inspection of Fig. 16 indicates that a redistribution of 30 kcal/mole from T' into V' has the dramatic effect of increasing by a factor of $\sim 10^3$ the rate of reaction in the endothermic direction (*58*, *80*).

In a few cases in other laboratories direct measurement has been made of the relative efficiency of vibration and translation in surmounting an energy barrier (*82–84*); in one of these cases (*84*) the barrier corresponded to a "substantially" (*44*) endothermic reaction; the reaction was $HF(v') + K \rightarrow H + KF$ (17 kcal/mole endothermic) and the effect of transferring 11 kcal/mole from reagent translation to vibration was to increase the reaction rate by a factor greater than 100.

The IR "chemiluminescence depletion" (CD) method, in which a prior reaction was used as a source of highly vibrationally excited reagent, was also used to obtain a measure of the efficiency of vibrational excitation in promoting endothermic reaction. Vibrational excitation was found to be highly efficient in carrying these reactions over their endothermic energy barriers (*85*, *86*).

The CD approach was also used to map out the dependence of reaction rate on reagent rotational excitation (*87*). There was an initial decline in reaction probability with increasing *J*, followed by a rise. Similar behavior has been noted in crossed-beam experiments (*88*, *89*).

Theory. We have found it revealing to link the preferred type of reagent energy distribution to the location of the energy barrier on the collinear PES. Figure 17 shows the dynamics characteristic of equal masses reacting across a PES with "early barrier" (surface I) and "late barrier" (surface II) (*90*). The effect of modest displacements of the barrier crest on the preferred mode of motion in the reagents was dramatic. On surface I a reagent translational energy only slightly in excess of the barrier height of 7 kcal/mole gave a calculable cross section, whereas a reagent vibrational energy double the barrier height gave a reactive cross section too small to be computed in our study. The converse behavior was found to apply on surface II.

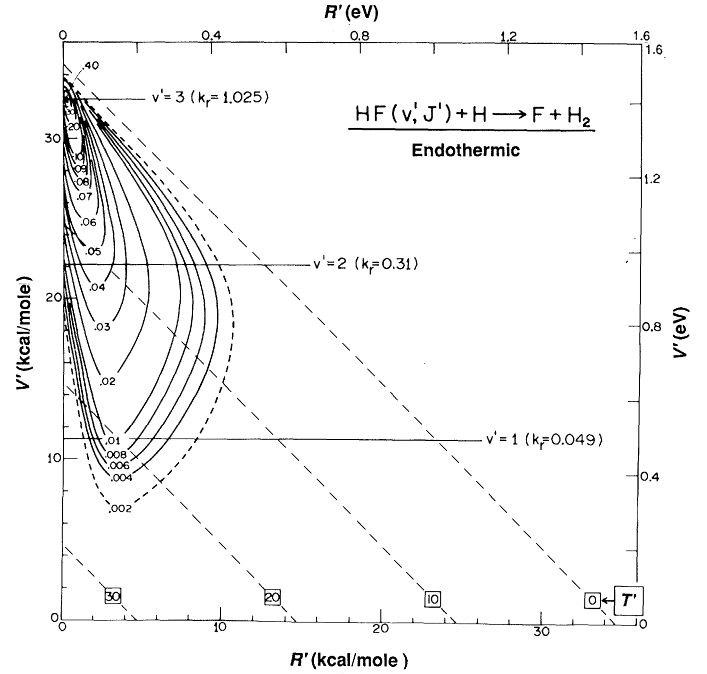

Fig. 16. Contours representing values of reagent vibrational, rotational, and translational energies for the endothermic reaction $HF(v',J') + H \rightarrow F + H_2$ which correspond to equal $k_r(\equiv k_{endo})$. The data were obtained by application of microscopic reversibility to the $k_f(\equiv k_{exo})$ given in Fig. 3. [Courtesy of *The Journal of Chemical Physics* (*80*)]

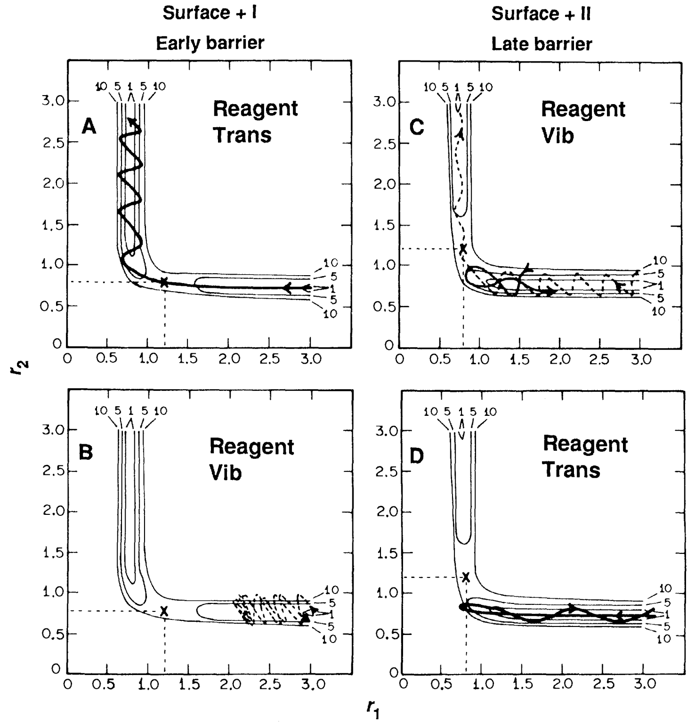

Fig. 17. (**A**) and (**B**) show specimen trajectories with (A) largely reagent translation ($T = 9$, $V = 0$) and (B) largely reagent vibration ($T = 1.5$ and $V = 14.5$) on an "early barrier" surface, that is, type I. (**C**) and (**D**) show trajectories with (C) largely reagent vibration ($T = 1.5$ and $V = 7.5$) and (D) largely reagent translation ($T = 16.0$, $V = 0$). All energies are in kilocalories per mole; reagent vibration is relative to $E(v = 0)$; the particles A, B, and C have equal mass. Positive and negative vibrational phases are shown with solid and broken lines, respectively. Barrier heights on both surfaces I and II are 7 kcal/mole; contours are labeled in kilocalories per mole. [Courtesy of *The Journal of Chemical Physics* (*90*)]

The correlations reduce to the proposition that a barrier predominantly along the coordinate of approach r_{AB} is best traversed by motion in that same coordinate, namely, reagent translation, whereas a barrier predominantly along the coordinate of separation r_{BC} is best traversed by motion in that coordinate, that is, vibration in the bond under attack. The trajectories in Fig. 17 (obtained by solution of the equations of motion, but capable of being pictured as the motion of a sliding mass across the PES) illustrate this; the reactive cases are (A) and (C) (early and late barriers) and the nonreactive cases are (B) and (D) (early and late barriers once again). The effect illustrated is sufficiently striking that it may also have relevance to the dynamics of reactions involving many atoms [see (*91*)], provided that these occur by a direct pathway.

The interest of these correlations is increased if we can link the form of the PES to the nature of the chemical reaction. Though unrecognized by reaction dynamicists, Hammond's postulate (*92*), namely, that for endothermic reactions the transition state resembles reaction products, might have pointed the way to the desired connection. Instead, a systematic study of a considerable number of exchange reactions $A + BC \rightarrow AB + C$ in terms of both the LEPS and the bond-energy bond-order (BEBO) methods led to the conclusion that for substantially exothermic reactions the barrier crest is located in the entrance valley (early barrier) of the PES, and for substantially endothermic reactions it is in the exit valley (late barrier) (*55*). From this, and the dynamical study of early and late barriers, it followed [as previously surmised (*93*)] that the favored degree of freedom for barrier crossing in substantially exothermic reactions would be translation, whereas reagent vibration would be most effective in giving rise to substantially endothermic reaction.

Future Directions

Two further approaches could assist in the quest for understanding of the choreography of chemical reaction. In the first, attempts are being made to observe the molecular partners while they are, so to speak, on the stage, rather than immediately before and after the reactive dance. This is reactive "transition state spectroscopy" (TSS); it is a young but burgeoning field of experimentation [for theory, see (*94*); for experiment, see (*95*)]. In the second approach the intention, stated a little grandiosely, is to have a hand in writing the script according to which the dynamics occurs; this is "surface aligned photochemistry" (SAP), in which the reagents are aligned by the forces at a crystal surface and held in a fixed arrangement immediately prior to the initiation of the reaction by light, thus restricting the subsequent pattern of motion. Some success has been achieved experimentally. In addition a trajectory study (*96*) has shown the simplified link between product attributes and reactive geometries that applies under the more disciplined conditions of restricted angle of approach and impact parameter characteristic of SAP.

Even in the world of molecules the civilizing influence of modest restraints is a cause for rejoicing.

REFERENCES AND NOTES

1. M. Beutler and M. Polanyi, *Z. Phys. Chem. B* **1**, 3 (1928); St. v. Bogdandy and M. Polanyi, *ibid.* **1**, 21 (1928); M. Polanyi and G. Schay, *ibid.*, p. 30.
2. D. R. Bates and M. Nicolet, *J. Geophys. Res.* **55**, 301 (1950).
3. G. Herzberg, *J. R. Astron. Soc. Can.* **45**, 100 (1951).
4. J. D. McKinley, D. Garvin, M. Boudart, *J. Chem. Phys.* **23**, 784 (1955); T. M. Cawthorn and J. D. McKinley, *ibid.* **25**, 583 (1956).
5. F. J. Lipscomb *et al.*, *Proc. R. Soc. London Ser. A* **233**, 455 (1956).
6. J. K. Cashion and J. C. Polanyi, *J. Chem. Phys.* **29**, 455 (1958).
7. ———, *ibid.* **30**, 1097 (1959); *Proc. R. Soc. London Ser. A* **258**, 529 (1960); *ibid.*, p. 564; *ibid.*, p. 570.
8. A. L. Schawlow and C. H. Townes, *Phys. Rev.* **112**, 1940 (1958); A. M. Prokhorov, *Zh. Eksp. Teor. Fiz.* **34**, 1658 (1958); *Sov. Phys. JETP* 7, 1140 (1958).
9. J. C. Polanyi, *Proc. R. Soc. Can.* **54(C)**, 25 (1960).
10. ———, *J. Chem. Phys.* **34**, 347 (1961).
11. ———, *Appl. Op. Suppl.* **2**, 109 (1965).
12. C. K. N. Patel, W. L. Faust, R. A. McFarlane, *Bull. Am. Phys. Soc.* **119**, 500 (1964); C. K. N. Patel and R. J. Kerl, *Appl. Phys. Lett.* **5**, 81 (1964); C. K. N. Patel, *Phys. Rev. Lett.* **12**, 588 (1964).
13. J. V. V. Kasper and G. C. Pimentel, *Phys. Rev. Lett.* **14**, 352 (1965); G. C. Pimentel, *Sci. Am.* **214**, 32 (April 1966).
14. P. E. Charters and J. C. Polanyi, *Discuss. Faraday Soc.* **33**, 107 (1962).
15. H. O. Pritchard, *ibid.*, p. 278.
16. J. C. Polanyi, *ibid.*, p. 279.
17. The film "Concepts in Reaction Dynamics" [prepared in collaboration with C. A. Parr and P. E. Charters (1970)] comes in 30- and 40-minute versions; it illustrates, with commentary, many of the types of dynamics discussed in this lecture. Copies of the film have been deposited in a number of countries. Inquiries should be made to the author at the University of Toronto.
18. K. G. Anlauf, P. J. Kuntz, D. H. Maylotte, P. D. Pacey, J. C. Polanyi, *Discuss. Faraday Soc.* **44**, 183 (1967).
19. P. D. Pacey and J. C. Polanyi, *J. Appl. Opt.* **10**, 1725 (1971).
20. D. H. Maylotte, J. C. Polanyi, K. B. Woodall, *J. Chem. Phys.* **57**, 1547 (1972).
21. K. G. Anlauf *et al.*, *ibid.*, p. 1561.
22. J. C. Polanyi and K. B. Woodall, *ibid.*, p. 1574.
23. J. C. Polanyi and J. J. Sloan, *ibid.*, p. 4988.
24. F. London, *Problem der Modernen Physik* (Sommerfeld Festschrift 1928), p. 104; *Z. Elektrochem.* **35**, 552 (1924).
25. H. Eyring and M. Polanyi, *Z. Phys. Chem. B* **12**, 279 (1931).
26. J. O. Hirschfelder and E. Wigner, *J. Chem. Phys.* 7, 616 (1929).
27. F. T. Wall, L. A. Hiller, J. Mazur, *ibid.* **29**, 255 (1958); *ibid.* **35**, 1284 (1961).
28. N. C. Blais and D. L. Bunker, *ibid.* **37**, 2713 (1962); *ibid.* **39**, 315 (1962).
29. J. C. Polanyi, in *Transfert d'Energie dans les Gaz*, R. Stoops, Ed. (Interscience, New York, 1962), pp. 177–182, 526–528; J. C. Polanyi and S. D. Rosner, *J. Chem. Phys.* **38**, 1028 (1963).
30. M. G. Evans and M. Polanyi, *Trans. Faraday Soc.* **35**, 178 (1939).
31. For a review, see B. S. Agrawala and D. W. Setser, in *Gas Phase Chemiluminescence and Chemi-ionization*, A. Fontijn, Ed. (Elsevier, New York, 1985), p. 157.
32. B. M. Berquist *et al.*, *J. Chem. Phys.* **76**, 2972 (1982); B. M. Berquist, L. S. Dzelzkalns, F. Kaufman, *ibid.*, p. 2984; L. S. Dzelzkalns and F. Kaufman, *ibid.* 77, 3508 (1982); *ibid.* **79**, 3836 (1983).
33. J. C. Weisshaar, T. S. Zwier, S. R. Leone, *ibid.* **75**, 4873 (1981); for a review, see C. E. Hamilton and S. R. Leone, in *Gas Phase Chemiluminescence and Chemi-ionization*, A. Fontijn, Ed. (Elsevier, New York, 1985), p. 139.
34. H. L. Welsh, C. Cumming, E. J. Stansbury, *J. Opt. Soc. Am.* **41**, 712 (1951); H. L. Welsh, E. J. Stansbury, J. Romanko, T. Feldman, *ibid.* **45**, 338 (1955).
35. N. Jonathan, C. M. Melliar-Smith, D. H. Slater, *Mol. Phys.* **20**, 93 (1971); N. Jonathan *et al.*, *ibid.* **22**, 561 (1971).
36. H. W. Chang and D. W. Setser, *J. Chem. Phys.* **58**, 2298 (1973); D. J. Bogan and D. W. Setser, *ibid.* **64**, 586 (1976).
37. J. C. Moehlmann and J. D. McDonald, *ibid.* **62**, 3061 (1975).
38. J. W. Hudgens and J. D. McDonald, *ibid.* **67**, 3401 (1977).
39. P. M. Aker, D. J. Donaldson, J. J. Sloan, *J. Phys. Chem.* **40**, 3110 (1986).
40. D. Brandt, L. W. Dickson, L. N. Y. Kwan, J. C. Polanyi, *Chem. Phys.* **39**, 189 (1979); L. W. Dickson, thesis, University of Toronto (1982).
41. J. H. Parker and G. C. Pimentel, *J. Chem. Phys.* **51**, 91 (1969); R. D. Coombe and G. C. Pimentel, *ibid.* **59**, 251 (1973); *ibid.*, p. 1535; M. J. Berry, *ibid.*, p. 6229.
42. D. M. Neumark, A. M. Wodtke, G. N. Robinson, C. C. Hayden, Y. T. Lee, *ibid.* **82**, 3045 (1985); D. M. Neumark *et al.*, *ibid.*, p. 3067.
43. R. B. Bernstein and R. D. Levine, *ibid.* **57**, 434 (1972); *Advances in Atomic and Molecular Physics* (Academic Press, New York, 1975), vol. 11; R. B. Bernstein and R. D. Levine, in *Modern Theoretical Chemistry*, vol. 3B of *Dynamics of Molecular Collisions*, W. H. Miller, Ed. (Plenum, New York, 1976), chap. 7.
44. D. S. Perry and J. C. Polanyi, *Chem. Phys.* **12,** 419 (1976).
45. K. G. Anlauf *et al.*, *J. Chem. Phys.* **53**, 4091 (1970).
46. H. Heydtmann and J. C. Polanyi, *J. Appl. Opt.* **10**, 1738 (1971).
47. M. A. Nazar, J. C. Polanyi, W. J. Skrlac, *Chem. Phys. Lett.* **29**, 473 (1974); J. C. Polanyi and W. J. Skrlac, *Chem. Phys.* **23**, 167 (1977).
48. D. Brandt and J. C. Polanyi, *ibid.* **35**, 23 (1978); *ibid.* **45**, 65 (1980).
49. L. T. Cowley, D. S. Horne, J. C. Polanyi, *Chem. Phys. Lett.* **12**, 144 (1971).
50. A. M. G. Ding, L. J. Kirsch, D. S. Perry, J. C. Polanyi, J. L. Schreiber, *Faraday Discuss. Chem. Soc.* **55**, 252 (1973).
51. J. C. Polanyi, J. L. Schreiber, W. J. Skrlac, *ibid.* **67**, 66 (1979).
52. J. C. Polanyi, *J. Quant. Spectros. Radiat. Transfer* **3**, 471 (1963).
53. P. J. Kuntz *et al.*, *J. Chem. Phys.* **44**, 1168 (1966).
54. D. S. Perry, J. C. Polanyi, C. Woodrow Wilson, Jr., *Chem. Phys.* **3**, 317 (1974).
55. M. H. Mok and J. C. Polanyi, *J. Chem. Phys.* **51**, 1451 (1969).
56. T. H. Dunning, Jr., *J. Phys. Chem.* **88**, 2469 (1984).
57. J. C. Polanyi, *Discuss. Faraday Soc.* **44**, 293 (1967).
58. For a review, see J. C. Polanyi, *Acc. Chem. Res.* **5**, 161 (1972).
59. For a review, see J. C. Polanyi and J. L. Schreiber, in *Kinetics of Gas Reactions*, vol. 6A of *Physical Chemistry—An Advanced Treatise*, H. Eyring, W. Jost, D. Henderson, Eds. (Academic Press, New York, 1974), p. 383.
60. P. J. Kuntz, E. M. Nemeth, J. C. Polanyi, *J. Chem. Phys.* **50**, 4607 (1969).
61. C. A. Parr, J. C. Polanyi, W. H. Wong, *ibid.* **58**, 5 (1973).
62. J. T. Muckerman, *ibid.* **54**, 1155 (1971); *ibid.* **56**, 2997 (1972); *ibid.* **57**, 3388 (1972).
63. J. C. Polanyi and J. L. Schreiber, *Chem. Phys. Lett.* **29**, 319 (1974).
64. ———, *Faraday Discuss. Chem. Soc.* **62**, 267 (1977).
65. C. F. Bender *et al.*, *Science* **176**, 1412 (1972).
66. H. F. Schaefer III, *J. Phys. Chem.* **89**, 5336 (1985).
67. P. J. Kuntz, M. H. Mok, J. C. Polanyi, *J. Chem. Phys.* **50**, 4623 (1969).
68. D. R. Herschbach, *Faraday Discuss. Chem. Soc.* **55**, 233 (1973).
69. M. G. Prisant, C. T. Rettner, R. N. Zare, *J. Chem. Phys.* **81**, 2699 (1984).
70. M. D. Pattengill and J. C. Polanyi, *Chem. Phys.* **3**, 1 (1974).
71. N. H. Hijazi and J. C. Polanyi, *J. Chem. Phys.* **63**, 2249 (1975); *Chem. Phys.* **11**, 1 (1975).

72. A. D. Walsh, *J. Chem. Soc.* **1953**, 2266 (1953).
73. J. J. Valentini, M. J. Coggiola, Y. T. Lee, *J. Am. Chem. Soc.* **98**, 853 (1976); *Faraday Discuss. Chem. Soc.* **62**, 232 (1977).
74. B. A. Blackwell, J. C. Polanyi, J. J. Sloan, *Chem. Phys.* **24**, 25 (1977).
75. D. L. Thompson, *J. Chem. Phys.* **56**, 3570 (1972).
76. J. C. Polanyi, *Faraday Discuss. Chem. Soc.* **55**, 389 (1973).
77. ——, J. L. Schreiber, J. J. Sloan, *Chem. Phys.* **9**, 403 (1975).
78. J. C. Polanyi, J. J. Sloan, J. Wanner, *ibid.* **13**, 1 (1976).
79. K. G. Anlauf, D. H. Maylotte, J. C. Polanyi, R. B. Bernstein, *J. Chem. Phys.* **51**, 5716 (1969).
80. J. C. Polanyi and D. C. Tardy, *ibid.*, p. 5717.
81. D. S. Perry, J. C. Polanyi, C. Woodrow Wilson, Jr., *Chem. Phys. Lett.* **24**, 484 (1974).
82. T. J. Odiorne, P. R Brooks, J. V. V. Kasper, *J. Chem. Phys.* **55**, 1980 (1971); J. G. Pruett, F. R. Grabiner, P. R Brooks, *ibid.* **63**, 3335 (1974); *ibid.*, p. 1173.
83. A. Gupta, D. S. Perry, R. N. Zare, *ibid.* **72**, 6237 (1980); *ibid.*, p. 6250.
84. F. Heismann and H. J. Loesch, *Chem. Phys.* **64**, 43 (1982).
85. D. J. Douglas, J. C. Polanyi, J. J. Sloan, *J. Chem. Phys.* **59**, 6679 (1973).
86. F. E. Bartoszek, B. A. Blackwell, J. C. Polanyi, J. J. Sloan, *ibid.* 74, 3400 (1981).
87. B. A. Blackwell, J. C. Polanyi, J. J. Sloan, *Chem. Phys.* **30**, 299 (1978).
88. H. H. Dispert, M. W. Geis, P. R. Brooks, *J. Chem. Phys.* 70, 5317 (1979).
89. M. Hoffmeister, L. Potthast, H. J. Loesch, *Book of Abstracts, Twelfth International Conference on the Physics of Electronic and Atomic Collisions* (Gatlinburg, 1981).
90. J. C. Polanyi and W. H. Wong, *J. Chem. Phys.* **51**, 1439 (1969).
91. M. H. Mok and J. C. Polanyi, *ibid.* **53**, 4588 (1970).
92. G. S. Hammond, *J. Am. Chem. Soc.* 77, 334 (1955).
93. J. C. Polanyi, *J. Chem. Phys.* **31**, 1338 (1959).
94. T. F. George, *J. Phys. Chem.* 86, 10 (1982), and references therein; A. M. F. Lau, *Phys. Rev. A* **13**, 139 (1976); *ibid.* **14**, 279 (1976); *Phys. Rev. Lett.* **43**, 1009 (1978); *Phys. Rev. A* **22**, 614 (1980); V. S. Dubov, L. I. Gudzenko, L. V. Gurvich, S. I. Yakovlenko, *Chem. Phys. Lett.* **45**, 330 (1977); S. I. Yakovlenko, *Sov. J. Quantum Electron.* 8, 151 (1977); A. E. Orel and W. H. Miller, *Chem. Phys. Lett.* **57**, 362 (1979); *J. Chem. Phys.* **70**, 4393 (1979); J. C. Light and A. Altenberger-Siczek, *ibid.*, p. 4108; J. C. Polanyi, *Faraday Discuss. Chem. Soc.* 67, 129 (1979); —— and R. J. Wolf, *J. Chem. Phys.* **75**, 5951 (1981); H. R. Mayne, R. A. Poirier, J. C. Polanyi, *ibid.* **80**, 4025 (1984); H. R. Mayne, J. C. Polanyi, N. Sathyamurthy, S. Raynor, *ibid.* 88, 4064 (1984); V. Engel, Z. Bacic, R. Schinke, M. Shapiro, *ibid.* **82**, 4844 (1985); V. Engel and R. Schinke, *Chem. Phys. Lett.* **122**, 103 (1985); P. M. Agrawal, V. Mohan, N. Sathyamurthy, *ibid.* **114**, 343 (1985).
95. P. Arrowsmith *et al.*, *J. Chem. Phys.* **73**, 5895 (1980); H. J. Foth, J. C. Polanyi, H. H. Telle, *J. Phys. Chem.* 86, 5027 (1982); P. Arrowsmith, S. H. P. Bly, P. E. Charters, J. C. Polanyi, *J. Chem. Phys.* **79**, 283 (1983); P. Hering, P. R. Brooks, R. F. Curl, Jr., R. S. Judson, R. S. Lowe, *Phys. Rev. Lett.* **44**, 657 (1980); P. R. Brooks, R. F. Curl, T. C. Maguire, *Ber. Bunsenges. Phys. Chem.* **86**, 401 (1982); H. P. Grieneisen, H. Xue-Jing, K. L. Kompa, *Chem. Phys. Lett.* **82**, 421 (1981); J. K. Ku, G. Inoue, D. W. Setser, *J. Phys. Chem.* **87**, 2989 (1983); T. C. Maguire, P. R. Brooks, R. F. Curl, J. H. Spence, S. Ulrick, *J. Chem. Phys.* **85**, 844 (1986); *Phys. Rev. A* **34**, 4418 (1986); P. D. Kleiber, A. M. Lyyra, K. M. Sando, S. P. Heneghan, W. C. Stwalley, *Phys. Rev. Lett.* **54**, 2003 (1985); P. D. Kleiber, A. M. Lyyra, K. M. Sando, V. Zafiropolos, W. C. Stwalley, *J. Chem. Phys.* **85**, 5493 (1986).
96. E. B. D. Bourdon *et al.*, *J. Phys. Chem.* **88**, 6100 (1984); E. B. D. Bourdon *et al.*, *Faraday Discuss. Chem Soc.* **82**, (1986).
97. The research described here insofar as it related to the work of this laboratory was performed over a 30-year period at the University of Toronto. It is a pleasure to express indebtedness to my colleagues at this university, most especially to the late D. J. LeRoy, who fostered this work from its inception, and to my students and postdoctoral associates whose talents, generosity, and friendship have made this undertaking possible and fulfilling.

Research Articles

A Small Viral RNA Is Required for in Vitro Packaging of Bacteriophage φ29 DNA

PEIXUAN GUO, STEPHEN ERICKSON, DWIGHT ANDERSON

A small RNA of *Bacillus subtilis* bacteriophage φ29 is shown to have a novel and essential role in viral DNA packaging in vitro. This requirement for RNA in the encapsidation of viral DNA provides a new dimension of complexity to the attendant protein-DNA interactions. The RNA is a constituent of the viral precursor shell of the DNA-packaging machine but is not a component of the mature virion. Studies of the sequential interactions involving this RNA molecule are likely to provide new insight into the structural and possible catalytic roles of small RNA molecules. The φ29 assembly in extracts and φ29 DNA packaging in the defined in vitro system were strongly inhibited by treatment with the ribonucleases A or T1. However, phage assembly occurred normally in the presence of ribonuclease A that had been treated with a ribonuclease inhibitor. An RNA of approximately 120 nucleotides co-purified with the φ29 precursor protein shell (prohead), and this particle was the target of ribonuclease action. Removal of RNA from the prohead by ribonuclease rendered it inactive for DNA packaging. By RNA-DNA hybridization analysis, the RNA was shown to originate from a viral DNA segment very near the left end of the genome, the end packaged first during in vitro assembly.

PROKARYOTIC RNA SPECIES HAVE BEEN CATEGORIZED INTO transfer RNA (tRNA), ribosomal RNA (rRNA), messenger RNA (mRNA), and small RNA groups, although some RNA species fit into more than one category (*1*). The heterogeneous small RNAs of approximately 200 nucleotides include regulators, enzymes, primers, fragments from processing reactions, and molecules of unknown function. For example, a 4.5*S* RNA is needed to develop or maintain ribosome function in the initiation of protein synthesis in *Escherichia coli* (*2*). We show here that a small RNA transcript of the *Bacillus subtilis* bacteriophage φ29 has a novel and essential function in viral DNA packaging. This RNA of approximately 120 nucleotides is not assembled into the mature virion but is a component of the precursor protein shell (prohead) into which the 18–kilobase pair (kbp) φ29 DNA–gene product 3 complex (DNA-gp3) is packaged during morphogenesis. This finding may have general significance because common mechanisms are used in packaging double-stranded DNAs of the tailed bacteriophages (*3*). In addition, the observation increases an awareness that molecules other than proteins may be involved in the assembly of DNA viruses. Indeed,, this role for RNA as a transient structural component and possible catalyst in viral morphogenesis extends the

---

Peixuan Guo is a graduate student, Stephen Erickson is a technician, and Dwight Anderson is a professor in the Departments of Microbiology and Dentistry, University of Minnesota, Minneapolis, MN 55455. The permanent address of Peixuan Guo is South China Agricultural University, Guangzhou (Canton), People's Republic of China.